Available online at www.sciencedirect.com

ScienceDirect

Green Energy & Environment 4 (2019) 121−126

www.keaipublishing.com/gee

Short communication

Degradation mechanism of tin phosphide as Na-ion battery negative electrode

Hiroyuki Usui [a,c], Yasuhiro Domi [a,c], Ryota Yamagami [b,c], Hiroki Sakaguchi [a,c,*]

[a] Department of Chemistry and Biotechnology, Graduate School of Engineering, Tottori University, 4-101 Minami, Koyama-cho, Tottori 680-8552, Japan

[b] Course of Chemistry and Biotechnology, Department of Engineering, Graduate School of Sustainability Science, Tottori University, 4-101 Minami, Koyama-cho, Tottori 680-8552, Japan

[c] Center for Research on Green Sustainable Chemistry, Tottori University, 4-101 Minami, Koyama-cho, Tottori 680-8552, Japan

Received 28 November 2018; revised 25 December 2018; accepted 4 January 2019
Available online 9 January 2019

Abstract

The degradation mechanism of an Sn_4P_3 electrode as Na-ion battery anode was investigated by using a transmission electron microscopic observation. At the first desodiation, we confirmed that Sn nanoparticles with 6 nm in size were dispersed in an amorphous-like P matrix. Compared to this, we observed aggregated Sn particles with sizes exceeding 50 nm after the drastic capacity fading. The capacity fading mechanism was for the first time confirmed to be Sn aggregation. To improve the capacity decay, we carried out the two kinds of charge−discharge cycling tests under the reduced volume changes of Sn particles and P matrix by limiting desodiation reactions of Na−Sn and Na_3P, respectively. The Sn_4P_3 electrode exhibited an excellent cyclability with the discharge capacity of 500 mA h g^{-1} for 420 cycles under the limited desodiation, whereas the capacity decay was accelerated under the limited sodiation. The results suggest that the Sn aggregation can be improved by the reduced volume change of the P matrix, and that it is very effective for improving anode performance of Sn_4P_3 electrode.

Keywords: Tin phosphide (Sn_4P_3); Ionic liquid electrolyte; Na-ion battery; Negative electrode material; Nanostructure

1. Introduction

Because of geographically localized Li resources, the prices of Li-ion batteries (LIBs) are expected to rise in the near future. A potential alternative to LIBs is Na-ion batteries (NIBs) because Na resources have a much lower cost compared with Li resources, and are not geographically localized. The development of NIB has been basically performed by referring to LIB mechanism because the properties of Na and Li are similar. In addition, NIB can operate by Na-insertion and Na-extraction into/from active materials of cathode and anode, while LIB similarly operates by Li-insertion and Li-extraction. However, not all active materials of LIB can react with Na ions. For instance, silicon (Si) is well known as a promising LIB anode material showing a very high theoretical capacity based on lithiation (alloying of Si with Li) and delithiation (dealloying of Li−Si). By contrast, a bulk form Si does not react with Na ions though a cluster-sized Si can react with Na ions [1]. Thus, the development of NIB active materials is separately required.

A conventional active material of NIB is hard carbon. A reversible capacity of approximately 300 mA h g^{-1} and a good

* Corresponding author. Department of Chemistry and Biotechnology, Graduate School of Engineering, Tottori University, 4-101 Minami, Koyama-cho, Tottori 680-8552, Japan.
E-mail address: sakaguch@tottori-u.ac.jp (H. Sakaguchi).

https://doi.org/10.1016/j.gee.2019.01.001

cyclability were achieved for hard carbon electrodes [2–4]. This cyclability is attributed to reversible Na-insertion into nanopore spaces of hard carbon. However, for the design of a high-energy density NIB, a much higher capacity is required for the anode active material. To meet this demand, many researchers have payed attention to some Na-active elements showing sodiation (alloying with Na) and desodiation (dealloying of Na). Phosphorus (P) and tin (Sn) are very attractive elements showing alloying–dealloying reactions. These elements have high theoretical capacities for fully sodiated compositions as Na_3P with 2596 mA h g^{-1} and $Na_{15}Sn_4$ ($Na_{3.75}Sn$) with 847 mA h g^{-1}. On the other hand, there are serious disadvantages for P and Sn. These elements show significant volume expansions of about 500% when fully sodiated. Owing to such significant volume expansion and contraction, active material layer of P and Sn produce the void space in itself, resulting in an electrode disintegration. In addition, a poor electronic conductivity of Na_3P phase limits the electrode reactions. Small Sn nanoparticles merge together to form large agglomerates, leading to an enhanced disintegration. Consequently, rapid capacities decay are observed for electrodes of P [5] and Sn [6].

To solve this problem, we have proposed the formation of compounds using other elements. We have newly produced various anode materials such as SnO [6], $LaSn_3$ [7], Sn_4P_3 [8–10], InP [11], GeP [11], and SiP [11]. Among them, Sn_4P_3 showed an outstanding performance in an ionic liquid electrolyte at room temperature not only with a high capacity over 750 mA h g^{-1} but also with a long cycle life of 200 cycles [9,10]. Based on transmission electron microscopic (TEM) observations and electrochemical characterizations, we have confirmed the origin of the excellent performance. Sn_4P_3 shows a phase separation reaction at the first cycle to form the nanostructure in which nanocrystalline Sn particles are dispersed in amorphous-like P matrix [9]. The aggregation of Sn particles can be suppressed because of this nanostructure. This excellent performance indicates the potential of Sn_4P_3 as NIB anode material. Mulder et al. also have reported an excellent cyclability of Sn_4P_3-based electrode [12]. However, a steep capacity fading is still observed after the 200th cycle [9,10]. Our previous TEM observations have been limited for the initial charge–discharge cycle. If the degradation mechanism after the 200th cycle is clarified, the performance can be further improved. In this study, we investigated the degradation mechanism of Sn_4P_3 electrode by using TEM observation, and tried to improve its cycling performance from the viewpoint of this mechanism.

2. Experimental section

Sn_4P_3 active material was prepared by a mechanical alloying (MA) method. The MA treatment carried out for a mixture of commercially available tin powder (99.99%, Rare Metallic) and red phosphorous powder (99.8%, Wako Pure Chemical) by using a Fritsch planetary-type high-energy ball mill (Fritsch Pulverisette P6) and a stainless steel vessel. The weight ratio of the mixture and stainless steel balls was 1:30. The MA duration time and rotation speed were 10 h and 380 rpm. The detailed procedure has been described in previous paper [9]. By the MA treatment, Sn_4P_3 with a trigonal crystal structure (Inorganic Crystal Structure Database, ICSD No. 03-066-0017) was successfully obtained. We prepared a slurry by using of Sn_4P_3/acetylene black/carboxymethyl cellulose/styrene-butadiene rubber with the weight ratio of 70/15/10/5 wt%. Film electrodes were obtained by coating of the slurry on Al foil current collector. The loading amount and the film thickness of active material layer were 1.2 mg cm^{-2} and 10 μm, respectively. Electrochemical measurements of sodiation (charge) and desodiation (discharge) were carried out for 2032-type coin half cells consisted of Na metal sheets and glass fiber separators. We used an ionic liquid electrolyte comprised of 1.0 mol dm^{-3} sodium bis(fluorosulfonyl)amide (NaFSA)-dissolved in *N*-methyl-*N*-propylpyrrolidinium bis(fluorosulfonyl)amide, abbreviated as Py13-FSA (C_3C_1pyrrFSA). Constant current charge–discharge tests were conducted using an electrochemical measurement system (HJ-1001 SM8A, Hokuto Denko Co., Ltd.) at 303 K with potential ranges of 0.005–2.000 V vs. Na^+/Na under the current density of 50 mA g^{-1}. This current density corresponds to 0.044 *C*-rate because the theoretical capacity of Sn_4P_3 is 1130 mA h g^{-1}. In the weight ratios of Sn and P in Sn_4P_3 are 84 and 16 wt%. Thus, the theoretical capacity of Sn_4P_3 is contributed by Sn of 972 mA h g^{-1} and P of 180 mA h g^{-1}.

The nanostructure of Sn_4P_3 active material after the capacity decay was observed by using a field-emission transmission electron microscope (HF-2000, Hitachi Ltd.). For the preparation of TEM sample, we carried out the charge–discharge cycling test for a film electrode consisting only of Sn_4P_3 powder and Al foil. This electrode was prepared by another technique, a gas-deposition method [13,14], and does not include any binder and conductive additive. This is very suitable for the fundamental evaluation of electrochemical reactions and the nanostructure analysis of active material after charge–discharge reactions. The TEM specimen was prepared by cleaving of active material layer from the surface of the cycled electrode after washing with organic solvent, and by putting the resulting small pieces on copper grid covered with amorphous carbon film.

3. Results and discussion

Fig. 1(a) and (b) show variation in discharge capacity and charge–discharge curves of Sn_4P_3 electrode cycled at the potential range of 0.005–2.0 V vs. Na^+/Na in ionic liquid electrolyte of NaFSA/Py13-FSA. In the charge curve at the first cycle, a potential shoulder was observed at around 1.0 V vs. Na^+/Na (Fig. 1(b)). It is suggested that FSA anions are cathodically decomposed to form a stable surface film composed of NaF [15], and that the surface film can suppress the cathodic decomposition of electrolyte in the subsequent cycle. The discharge capacity was gradually increased for the

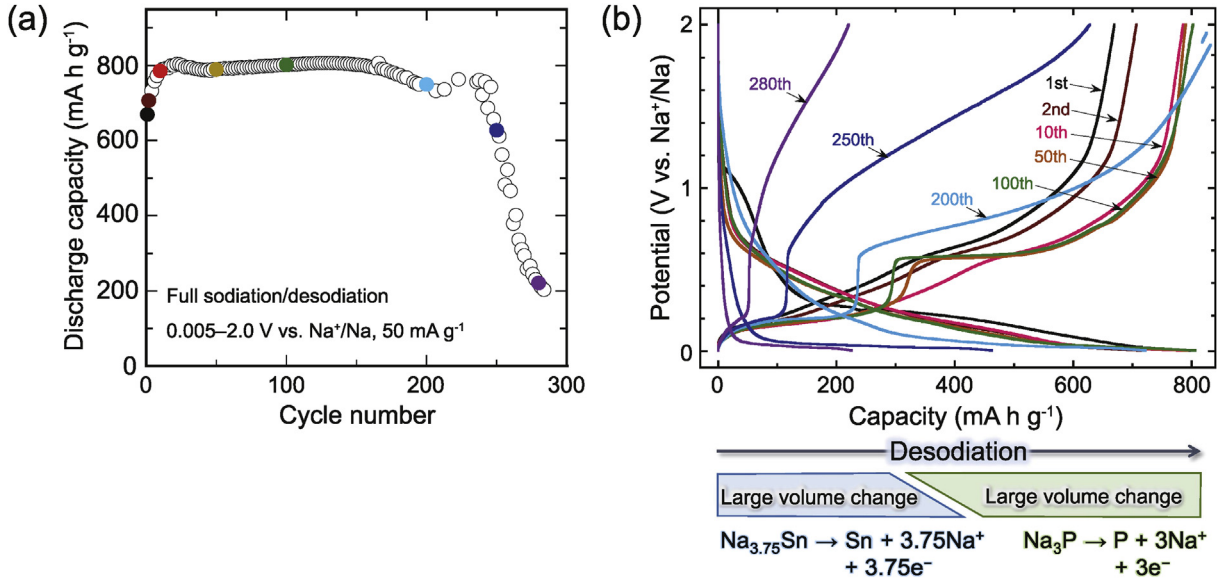

Fig. 1. (a) Cycling performance of Sn_4P_3 electrode tested in ionic liquid electrolyte (NaFSA/Py13-FSA). (b) Dependence of its charge–discharge curves on cycle number. Colors of charge–discharge curves correspond to those of plots in cyclic performance.

initial 10 cycles (Fig. 1(a)). This suggests that the phase separation of Sn_4P_3 completed for the initial 10 cycles. In the discharge curves after the 50th cycle, two potential plateaus clearly appeared (Fig. 1(b)). The potential plateaus at 0.1 and 0.5 V vs. Na^+/Na basically originate from desodiation reactions of $Na_{3.75}Sn$ ($Na_{15}Sn_4$) [16,17] and Na_3P [18,19], respectively, though residual desodiation reactions of Na−Sn ($NaSn \rightarrow NaSn_3 \rightarrow Sn$) slightly occurred at 0.55 and 0.70 V vs. Na^+/Na [7]. The length of potential plateau at around 0.5 V vs. Na^+/Na is larger than the contributed theoretical capacity (180 mA h g^{-1}) of P in Sn_4P_3, which is possibly caused by the residual desodiation reactions of Na−Sn and a side reaction such as electrolyte decomposition. At the 200th cycle, the desodiation plateau of Na_3P was gradually inclined, and shifted toward higher potential. After this cycle, we sometimes observed anomalous discharge reactions. After the 240th cycle, the capacity drastically decayed. To reveal the origin of the performance degradation after 200 cycles, TEM observations were performed for the Sn_4P_3 active material after the capacity decay.

Fig. 2 displays TEM images of Sn_4P_3 particles at the first cycle and after the capacity fading (corresponding to 280 cycle). At the desodiation state of the first cycle (Fig. 2(a)), we can recognize particles with size of about 6 nm. Our previous study has revealed that the particles are nanocrystalline Sn produced by the phase separation of Sn_4P_3, and that those are well dispersed in amorphous-like P matrix [9]. After the capacity fading (Fig. 2(b)), significantly larger particles were observed. Some particles showed the sizes exceeding 50 nm. The corresponding selected area electron diffraction demonstrated the existence of crystallized Sn. Based on these clear evidence of TEM results, we directly confirmed for the first time the Sn aggregation as the origin of capacity degradation. We are herewith suggesting that Sn aggregation slowly

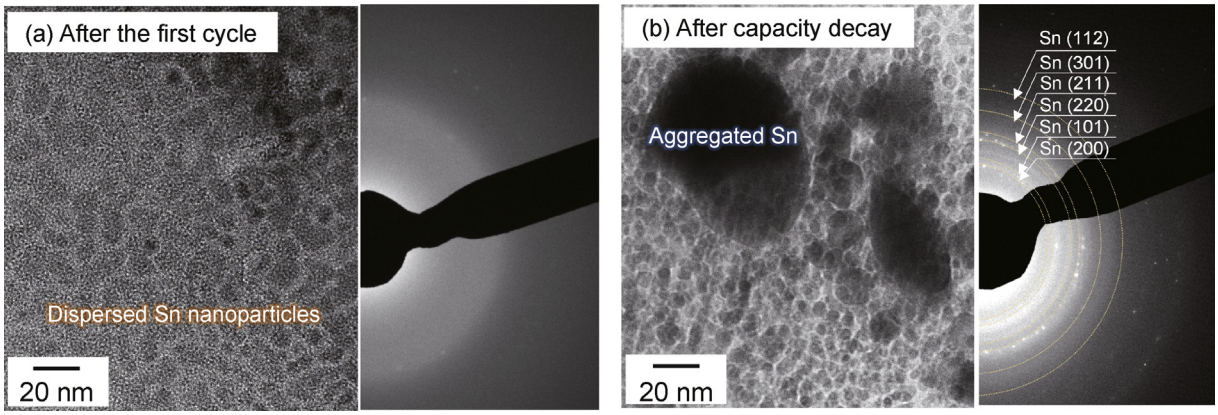

Fig. 2. TEM images and selected area electron diffractions of desodiated Sn_4P_3 particle (a) after the first cycle and (b) after capacity decay.

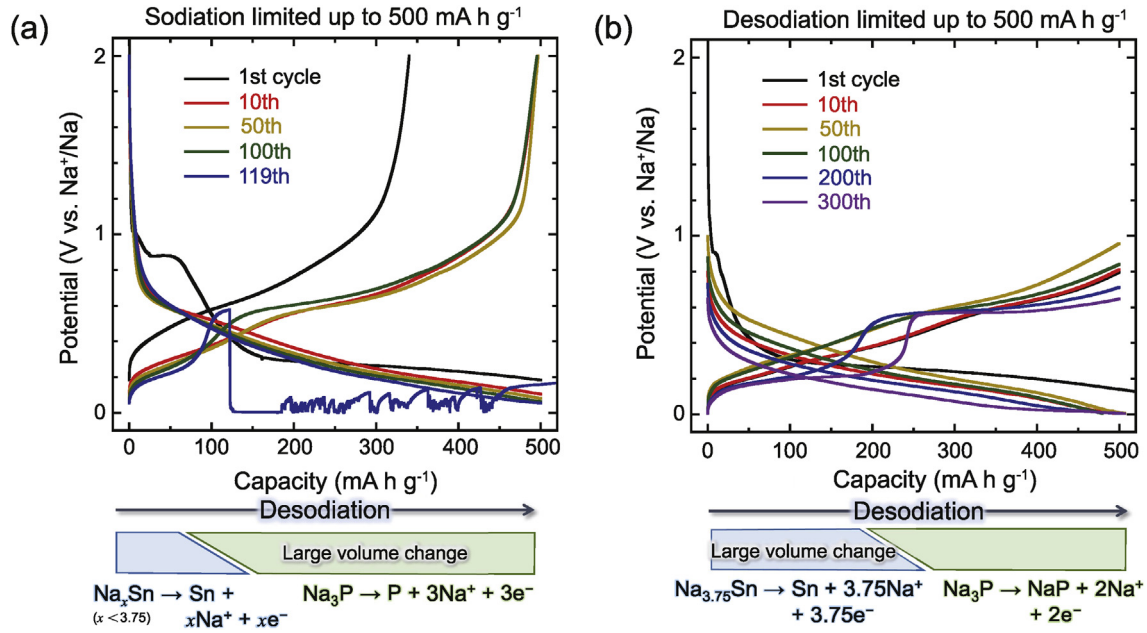

Fig. 3. Charge–discharge curves of Sn_4P_3 electrodes cycled at capacity limitations (a) for sodiation process and (b) for desodiation process.

progressed by the repeated volume changes for a long cycle, and that it reached a critical stage at around the 200th cycle to begin the capacity fading. To improve the cyclability, P matrix should suppress the Sn aggregation more sufficiently. However, P also shows large volume changes up to 490% during phase transformations between P and Na_3P. As an approach to solve this problem, we conceived a new scheme of charge–discharge reactions with reduced volume changes of Sn particles or P matrix. If the sodiation capacity is limited up to 500 mA h g^{-1}, the volume changes of Sn particle can be suppressed because the Sn's sodiation is not completed owing to the preceding P's sodiation with the contributed theoretical capacity of 180 mA h g^{-1} in Sn_4P_3. On the other hand, if the desodiation reaction is stopped up to 500 mA h g^{-1}, the phase transformation from Na_3P to P is suspended, resulting in the reduced volume change of P matrix. Therefore, by the capacity limitations for sodiation and desodiation, we can investigate the influence of suppressed volume changes for Sn and P, respectively.

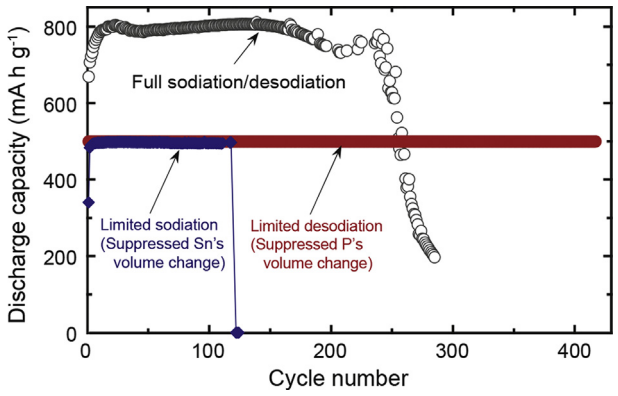

Fig. 4. Cycling performances of Sn_4P_3 electrodes under capacity limitations for sodiation process and for desodiation process.

Fig. 3 compares charge–discharge curves of Sn_4P_3 electrode cycled at capacity limitations for sodiation process and desodiation process. When the sodiation capacity was limited, the curve profiles by the 10th cycle were similar to those at the full sodiation/desodiation reactions (Fig. 1(b)). At the 100th cycle, the desodiation plateaus of Na_xSn and Na_3P began to appear. However, an anomalous discharge reaction was observed at around the 119th cycle. It is suggested that Sn aggregation was accelerated by the sodiation capacity limitation, resulting in an internal short circuit between the electrode and Na counter electrode. The charge–discharge cycling test was stopped by the anomalous discharge. In contrast, no anomalous discharge reaction was observed for 300 cycles under the desodiation capacity limitation (Fig. 3(b)). After the 200th cycle, the desodiation plateaus of $Na_{3.75}Sn$ and Na_3P became clear. Marbella et al. have recently reported that a stable Na_3P phase persists during desodiation until 0.6 V vs. Na^+/Na, and that the phase transformation from Na_3P to NaP takes place at around 0.6 V vs. Na^+/Na [20]. In this study, the desodiation was finished in the potential range of 0.6–1.0 V vs. Na^+/Na, indicating the formation of an intermediate Na–P phase, NaP (Fig. S1). By the phase transformation between Na_3P and NaP, the volume changes will be decreased from 490% to 216% compared with that between Na_3P and P (Fig. S2). On the other hand, the sodiation was finished in the potential range of 0.1–0.05 V vs. Na^+/Na as shown in Fig. 3(a). This indicates the phase transformations between Sn and NaSn or between Sn and Na_9Sn_4. These phase

transformations produce volume changes of 220% and 348%, which are much smaller than the volume change of 524% when Sn forms $Na_{15}Sn_4$ (Fig. S3).

Fig. 4 shows the cycling performances of the electrodes under capacity limitations for sodiation process and for desodiation process. In the case of the limited sodiation, the cycling test was stopped at the 119th cycle though the capacity was maintained by this cycle. On the other hand, the discharge capacity of 500 mA h g^{-1} was maintained for 420 cycles in the charge−discharge test with the limited desodiation. These results clearly indicate that the degradation mechanism of Sn_4P_3 electrode is the Sn aggregation insufficiently suppressed by P matrix, and that it can be improved by the reduced volume change of the matrix during desodiation reaction of P. The capacity decay was accelerated under the limited sodiation in spite of the suppressed volume change of Sn, which demonstrating that volume suppression of P matrix is much more critical than that of Sn nanoparticles. This new finding is very valuable for developing Sn_4P_3-based materials as advanced anode materials of NIB.

4. Conclusions

In this study, the degradation mechanism of Sn_4P_3 electrode as NIB anode was investigated by using TEM observation. After the desodiation of the initial cycle, it was confirmed that Sn nanoparticles with 6 nm in size were dispersed in amorphous-like P matrix. After the drastic capacity fading, we observed aggregated Sn particles with sizes exceeding 50 nm. The capacity fading mechanism was for the first time confirmed to be Sn aggregation by the clear evidence of this TEM observation. To improve the capacity decay, we carried out the two kinds of charge−discharge cycling tests under the reduced volume changes of Sn particles and P matrix by limiting desodiation reactions of Na−Sn and Na_3P, respectively. The Sn_4P_3 electrode exhibited an excellent cyclability with the discharge capacity of 500 mA h g^{-1} for 420 cycles under the limited desodiation, whereas the capacity decay was accelerated under the limited sodiation. The results suggest that the Sn aggregation can be improved by the reduced volume change of the P matrix, and that it is very effective for improving anode performance of Sn_4P_3 electrode.

Conflict of interest

All authors declare that: (i) no support, financial or otherwise, has been received from any organization that may have an interest in the submitted work; and (ii) there are no other relationships or activities that could appear to have influenced the submitted work.

Acknowledgment

This study was partially supported by Advanced Low Carbon Technology Research and Development Program (ALCA, 16200610802), Joint Usage/Research Program on Zero-Emission Energy Research, Institute for Applied Ecology, Kyoto University (ZE29A-14, ZE30A-05, ZE30A-06), and Japan Society for the Promotion of Science (JSPS) KAKENHI (Grant Number 17H03128, 17K17888, 16K05954). A part of this work was supported by "Advanced Characterization Nanotechnology Platform, Nanotechnology Platform Program of the Ministry of Education, Culture, Sports, Science and Technology (MEXT), Japan" at the Research Center for Ultra-High Voltage Electron Microscopy in Osaka University (A-17-OS-0020, A-18-S-0002). The authors thank Prof. H. Yasuda and Dr. T. Sakata for their helpful assistances in HR-TEM observations.

Appendix A. Supplementary data

Supplementary data to this article can be found online at https://doi.org/10.1016/j.gee.2019.01.001.

References

[1] M. Shimizu, H. Usui, K. Fujiwara, K. Yamane, H. Sakaguchi, J. Alloy. Compd. 640 (2015) 440–443.
[2] S. Komaba, W. Murata, T. Ishikawa, N. Yabuuchi, T. Ozeki, T. Nakayama, A. Ogata, K. Gotoh, K. Fujiwara, Adv. Funct. Mater. 21 (2011) 3859–3867.
[3] M. Dahbi, T. Nakano, N. Yabuuchi, T. Ishikawa, K. Kubota, M. Fukunishi, S. Shibahara, J.-Y. Son, Y.-T. Cui, H. Oji, S. Komaba, Electrochem. Commun. 44 (2014) 66–69.
[4] M. Dahbi, M. Kiso, K. Kubota, T. Horiba, T. Chafik, K. Hida, T. Matsuyama, S. Komaba, J. Mater. Chem. A 5 (2017) 9917–9928.
[5] M. Shimizu, H. Usui, K. Yamane, T. Sakata, T. Nokami, T. Itoh, H. Sakaguchi, Int. J. Electrochem. Sci. 10 (2015) 10132–10144.
[6] M. Shimizu, H. Usui, H. Sakaguchi, J. Power Sources 248 (2014) 378–382.
[7] H. Usui, Y. Domi, S. Ohshima, H. Sakaguchi, Electrochim. Acta 246 (2017) 280–284.
[8] H. Usui, T. Sakata, M. Shimizu, H. Sakaguchi, Electrochemistry 83 (2015) 810–812.
[9] H. Usui, Y. Domi, K. Fujiwara, M. Shimizu, T. Yamamoto, T. Nohira, R. Hagiwara, H. Sakaguchi, ACS Energy Lett. 2 (2017) 1139–1143.
[10] H. Usui, Y. Domi, H. Nishida, K. Yamaguchi, R. Yamagami, H. Sakaguchi, ChemistrySelect 3 (2018) 8462–8467.
[11] H. Usui, Y. Domi, R. Yamagami, K. Fujiwara, H. Nishida, H. Sakaguchi, ACS Appl. Energy Mater. 1 (2018) 306–311.
[12] Y. Xu, B. Peng, F.M. Mulder, Adv. Energy Mater. 8 (2018) 1701847.
[13] H. Sakaguchi, T. Toda, Y. Nagao, T. Esaka, Electrochem. Solid-State Lett. 10 (2007) J146–J149.
[14] H. Usui, Y. Kiri, H. Sakaguchi, Thin Solid Films 520 (2012) 7006–7010.
[15] M. Dahbi, M. Fukunishi, T. Horiba, N. Yabuuchi, S. Yasuno, S. Komaba, J. Power Sources 363 (2017) 404–412.
[16] L.D. Ellis, T.D. Hatchard, M.N. Obrovac, J. Elecreochem. Soc. 159 (2012) A1801–A1805.

[17] Z. Du, R.A. Dunlap, M.N. Obrovac, J. Alloy. Compd. 617 (2014) 271–276.
[18] M. Shimizu, Y. Tsushima, S. Arai, ACS Omega 2 (2017) 4306–4315.
[19] M. Mortazavi, Q. Ye, N. Birbilis, N.V. Medhekar, J. Power Sources 285 (2015) 29–36.
[20] L.E. Marbella, M.L. Evans, M.F. Groh, J. Nelson, K.J. Griffith, A.J. Morris, C.P. Grey, J. Am. Chem. Soc. 140 (2018) 7994–8004.